Fabrication, Characterization, and Gas Sensing Properties of Different Semiconductor Metal Oxide Nanostructures for LPG Detection: A Comparative Study

A.H.M.N.N. Bandara [a]*, G.K.R. Senadeera [a, b], K.N.D. Bandara [a], and V.P.S. Perera [a]

[a] Department of Physics, Faculty of Natural Sciences, The Open University of Sri Lanka, 10250
[b] National Institute of Fundamental Studies, Sri Lanka, 20000
*doneranji@gmail.com , gksen@ou.ac.lk , knban@ou.ac.lk , vpper@ou.ac.lk

ABSTRACT

The research explores how the structural, morphological, and electrical properties of nanostructured semiconductor metal oxides (SMOs), including Cu2O, ZnO, TiO2, and reduced graphene oxide (rGO), synthesized via electrochemical deposition and doctor blading techniques, influence their effectiveness in sensing liquid petroleum gas (LPG). Scanning electron microscopy (SEM) and X-ray diffraction (XRD) analysis were used to assess the chemical composition and structure. Cu2O, ZnO, and TiO2 were found to exhibit significant polycrystalline structures, with increasing average crystallite sizes of approximately 42.8 nm, 70.1 nm, and 87.78 nm, respectively. The dominant (111) Cu2O phase displayed a homogeneous cuboid morphology. rGO exhibited a single-plane (002) microstructure with a crumpled paper texture and an average crystallite size of ~85.3 nm, indicating a successful hydrothermal reduction of graphene oxide (GO). UV-vis absorption spectra in the range of 200 – 800 nm revealed the presence of different energy bands in ZnO, TiO2, and rGO, alongside their major band energies of 3.2 eV, 3.3 eV, and 1.9 eV. Cu2O thin films, with the lowest band energy gap of 2.5 eV, exhibited high photocatalytic activity, potentially enhancing chemical reaction rates during gas sensing under light exposure. Additionally, alternating current (AC) impedance spectra of SMO indicated increased film conductivities with positive bias voltages. ZnO films showed the most significant gas response (~27%) for LPG sensing at 70 °C, with response and recovery times of less than 20 seconds. A stable and considerably high LPG sensitivity of ~11% was discovered with Cu2O. This finding underscores the significance of its relatively small grain size in influencing its sensitivity to LPG.

KEYWORDS: *Semiconductor metal oxides (SMO), Thin films, Surface morphology, Liquid petroleum gas (LPG)*

1 INTRODUCTION

Airborne pollutants arise from various anthropogenic and natural sources, significantly impacting indoor and outdoor environments. Common anthropogenic sources include combustion processes in household appliances, vehicles, and industrial machinery. Additionally, wildfires contribute to air pollution through the release of combusted organic matter. These processes emit a multitude of toxic gases, including hydrogen sulfide, carbon monoxide, methane, other hydrocarbons (e.g. LPG), ammonia, and chlorine. Importantly, the severity of health effects associated with air pollution is not entirely dependent on the concentration. Even minute quantities of certain toxic gases, such as hydrogen sulfide and carbon monoxide, can be lethal and cause poisoning or asphyxiation.

Liquefied petroleum gas (LPG) is a mixture of hydrocarbon gases, primarily propane and butane, but this specific ratio varies depending on the intended use. It is a versatile fuel source with a range of applications such as heating, cooking, and transportation. While LPG offers many benefits, it is important to remember that LPG vapor is highly flammable and can readily ignite, posing fire hazards. Also in high concentrations, LPG displaces oxygen, leading to potential suffocation risks.

But, in high concentrations, LPG vapor is considered an anesthetic, ignitable, and asphyxiating agent. Therefore, there is an urgent need for fast and selective early detection of LPG leakage to prevent accidental explosions and other side effects. There is a considerable amount of research done on new approaches to LPG gas sensing. This takes effect as a resistance change in the surface layers of the

https://doi.org/10.54389/YTCT4469

developed sensing material as it interacts with the leaked gas molecules. It is then converted into an electrical signal which indicates the leakage. Generally, traditional sensing devices depend on the adsorption and desorption of oxygen molecules in the environment.

To improve the effectiveness of traditional resistive metal oxide sensors with growing challenges such as low selectivity to particular gases and high operating temperatures, leading to increased power usage, shorter sensor lifespan, and less portability has to be addressed. Despite the widespread use of metal oxides in gas sensors, a fresh strategy is essential to enhance both selectivity and sensitivity at room temperature.

Semiconducting metal oxide (SMO) gas sensors come in various types, each with its film-synthesized method and mechanism for detecting specific gases. Selecting a particular SMO type depends on the targeted gas, sensitivity requirements, and the intended application (Chen et al., 2020; Kalubowila et al., 2019; Shishiyanu et al., 2005; Siripala et al., 1989). There is much research to improve the sensing mechanism using different SMO materials. A wide number of metal-oxides for example, SnO_2, In_2O_3, Fe_2O_3, ZnO, WO_3, TiO_2, Cu_2O, Cr_2O_3, Co_3O_4, V_2O_5, CuO, etc. have been investigated for different target gases with varying degrees of success (Bandara et al., 2017; Barreca et al., 2007; Han et al., 2012; Liao et al., 2009; Miremadi et al., 1994) However, most of these metal-oxide gas sensors perform at high temperatures, which often limits their usage for this type of detection.

Titanium dioxide (TiO_2) is a material that holds significant importance due to its unique physical and optical properties. These properties include a high melting point, resistance to chemical reactions, efficient light absorption and stability, and rapid electron movement. Recently, scientists have explored combining TiO_2 with graphene (Garrafa-Gálvez et al., 2019; Ibrayev et al., 2019; Wang et al., 2013) to improve its photocatalytic performance. Graphene oxide (GO) is a popular precursor material for synthesizing graphene due to its ease of production and large-scale availability. However, GO has a very different microstructure than pure graphene because of the presence of oxygen-containing groups. These groups significantly reduce the electrical conductivity of GO. Researchers have successfully addressed this issue by chemically reducing GO to produce reduced graphene oxide (rGO). This process is cost-effective, allows for large-scale production, and enables the creation of rGO with a surface that can form composites with various materials, including TiO_2.

Yet again, Zinc oxide (ZnO) stands out as a promising material for gas sensors (2009; Choi et al., 2021; Kuwabara et al.,) development due to its attractive combination of properties such as non-toxicity, affordability, and readily available precursors. Its direct band gap of 3.37 eV and substantial exciting binding energy of 60 meV at room temperature make it particularly interesting for photocatalytic applications as well. Cu_2O stands out for its ease of fabrication, low fabrication costs and processing temperatures, high deposition rates, and controlled crystallization, particularly when producing large-area thin films. These attributes position Cu_2O as a promising candidate for cost-effective gas sensors, photo-electrochemical cells, and catalytic applications.

The difference in deposition/fabrication technique employed or the conditions supplied throughout the process also has shown a positive impact on the performance of a sensor. Most importantly the initial form of the SMO which is taken as an electrolyte, a paste, or as a solid could decide all the above-mentioned sensing parameters such as grain size, film thickness, and surface free energy. In the sense of electrolyte-based depositions, conditions such as pH, temperature, number of cycles, deposition period, working/reference electrode, and substrate used to deposit, were reported to be the deciding factors.

This paper reports on the comparative study of different SMOs and their characteristics utilized for LPG sensing. It conducts a detailed structural, morphological, and wettability investigation of Cu_2O, ZnO, TiO_2, and rGO films synthesized via electrochemical deposition and doctor blading techniques. In addition, the optical-electrical characteristics of the above films were investigated by means of UV visible absorption, and AC impedance spectroscopy. This study also emphasizes such characterizations that will enable optimizing the selected film parameters for using them as efficient liquid petroleum gas sensing platforms.

2 MATERIALS AND METHODS

To ensure the elimination of impurities on the FTO interface, the substrates were pre-cleaned with detergent, subjected to ultrasonic agitation for 10 minutes with distilled water, and further treated by boiling in isopropyl alcohol (99.9%) at 80 ℃.

2.1 Synthesis of ZnO and Cu_2O: Electrochemical Deposition

An FTO glass substrate was used to deposit the ZnO and Cu2O films which were placed as the working electrode in a three-electrode electrochemical cell with Ag/AgCl reference electrode and platinum counter electrode. Here, an area of ~ 1×1.5 cm2 of the FTO glass was immersed in the aqueous electrolyte solution consisting of a mixture of 3.5 M lactic acid (Sigma–Aldrich, purity - 99.0%) and 0.45 M cupric sulfate (Sigma–Aldrich, purity - 99.0%). The electrolyte solution was adjusted to a pH of 10 using a calibrated EUTECH PC 2700 scientific pH meter. This was achieved by adding saturated sodium hydroxide (NaOH) drop wise. Then it was maintained at a constant temperature of 60°C throughout the deposition process by placing the chemical cell inside a 60 °C water bath under continuous magnetic stirring. A potentiostatic electrochemical deposition was employed with - 450 mV potential across the Ag/AgCl reference electrode and the FTO substrate (Miremadi et al., 1994), for 30 min duration to obtain optimum film thickness and surface morphology. The electrochemical deposition of ZnO occurred in a two-electrode chemical cell containing a 0.1 M Zn(NO3)2 aqueous electrolyte solution (~pH 5) and graphite counter electrode. Under a constant temperature of 60 °C and a constant potential difference of -2.00 V, the deposition was carried out for 1 hour under vigorous stirring. After the deposition, all the films were washed with distilled water, then treated with heat for 30 minutes at 60 °C, and allowed to settle in the air at room temperature.

2.2 Fabrication of rGO and TiO_2 films: Doctor blading

Here, the Graphite oxide (GO) was initially synthesized using the modified Hummers method. For that, 1 g of natural graphite and 0.5 g of NaNO3 were finely ground to a powder and added to 25 ml of concentrated H2SO4 maintained at 0 ℃ in an ice bath with vigorous stirring. Subsequently, 3 g of KMnO4 was slowly introduced into the mixture while stirring at temperatures below 20 ℃ for 3 hours. Following this, deionized water was gradually added in two portions of 50 ml and 100 ml at 50 ℃, along with 5 ml of 30% H2O2 added drop wise until the reaction with KMnO4 was completed. The resulting GO precipitate was separated via centrifugation, wherein it underwent three cycles of washing with 5% HCl and deionized water to eliminate metallic ions. The GO was then dried in an oven at 250 ℃ for 30 minutes and subsequently hydrothermally reduced to obtain Reduced Graphene Oxide (rGO). The synthesized rGO, obtained in powder form, was stored in a sealed compartment to prevent moisture absorption. To fabricate rGO and TiO2 films, fine powders of each sample were manually ground in a mortar for 25 minutes at room temperature. During the grinding process, 1 ml of 0.1 M HNO3, 1 drop of Triton X-100, and polyethylene glycol (PEG-400) were sequentially added to ensure the formation of homogeneous clear pastes of rGO and TiO2. Subsequently, these pastes were uniformly grafted onto a cleaned FTO substrate on an area of 2 cm2, resulting in films with an approximate thickness of 0.06 mm (thickness of the scotch tape) using the doctor blading method. The grafting process occurred at a constant temperature of 70 ℃. Finally, the films were sintered in a furnace at 450 ℃ for 45 minutes to enhance their structural integrity and stability.

2.3 Film characterization

The surface structures and morphologies of the SMO films were investigated using high energy X-ray diffraction (XRD, Regaku Ultima–IV) pattern taken with Cu-Kα (λ=1.5418 Å) as the source of X- rays in the 200-800 2Θ range. Surface morphologies of as prepared films were characterized via scanning electron micrographs (SEM, Zeiss EVO 15 LS), and the electrical characterization was conducted by AC impedance spectroscopic Nyquist plots using AUTOLAB Model PGSTAT 302 potentiostat/galvanostat using three-electrode electrochemical cell containing Cu2O deposited FTO substrate as the working electrode, platinum counter electrode, and Ag/AgCl as the reference electrode in 0.1 M NaAc electrolyte. The optical energy band gaps were characterized using the UV-visible spectrophotometer (Genesys 10s UV-Vis).

3 RESULTS AND DISCUSSION

3.1 Surface Structure and Morphological Characteristics

The fabricated films were subjected to SEM and XRD analysis to recognize the suitability of the surface structural and morphological features of the SMO for LP gas sensing applications. This was analyzed based on the visible surface roughness, pore density, grain size, and distribution. Fig. 1 (a-d) and 1(e-f) illustrate the top SEM images of Cu2O, ZnO, TiO2, and rGO film surfaces in 200 nm scale and their XRD spectra respectively. As in, the overall comparison of surface areas (Fig. 1a-d) which facilitate the gaseous adsorption rate indicates a possible high LPG adsorption rate with Cu2O (Fig. 1a) due to its high surface area. Moreover, the high inter-particle porous nature (Fig. 1b) distinguished in ZnO reveals its ability to respond to gases even at low concentrations and low operating temperatures (Choi et al., 2021). Fig. 1c shows comparatively smaller (< 200 nm) nanoparticles to be aggregated in the titanium dioxide film whilst Graphene oxide has a layered structure, which is formed by separate sheets. Reduced graphene oxide sheets tend to form "wrinkles" and folds, as seen in Fig. 1d.

Fig.1 (e-f) shows the XRD patterns of Cu2O and ZnO electro-chemically deposited (ECD) on FTO substrates. The specific homogeneous, compact, and cuboid structure seen in SEM images (Fig. 1a) of Cu2O could be attributed to the substantially high peak intensity of (111) Cu2O plane observed amongst (110), (200), (211), and (220) orientations with comparatively low intensities of substrate (JCPDS card no. 05-0667). The high intensities of several diffraction peaks in Fig. 1f indicate that the samples were highly crystalline yet showed no specific crystal shape like Cu2O, but a homogeneous grain-like distribution followed by the standard pattern of crystalline ZnO (JCPDS File No. 36–1451).

The presence of different intensity orientations indicates a polycrystalline nature in the fabricated Cu2O, ZnO, and TiO2 films. Unassigned smaller peaks identified in these XRD spectra correspond to the FTO substrate (JCPDS card no. 77-0447). Figure 1 (g-h) shows the XRD analysis of TiO2 and rGO films. As can be seen with TiO2 nanoparticles (Fig. 1g), the 2θ peaks at 25.3˚, 37.8˚, 48.0˚, 53.9˚, 55.1˚, 62.7˚, can be indexed as (101), (004), (200), (105), (211), and (204) crystal planes of anatase TiO2 (JCPDS card no. 21-1272). On the other hand, Fig 1h depicts the complete reduction of graphite oxide into reduced graphene as an absence of the characteristic peak of graphite oxide generally observed at $2\theta \approx 11°$, and the presence of rGO peak at ($2\theta \approx$) 26°.

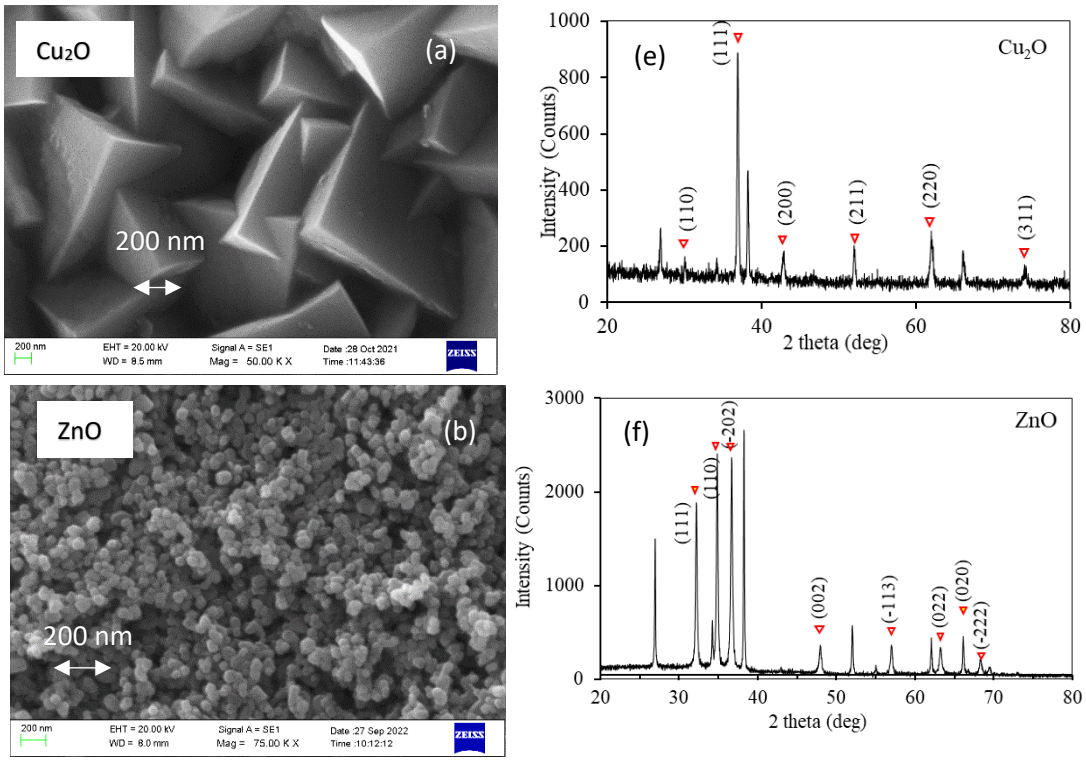

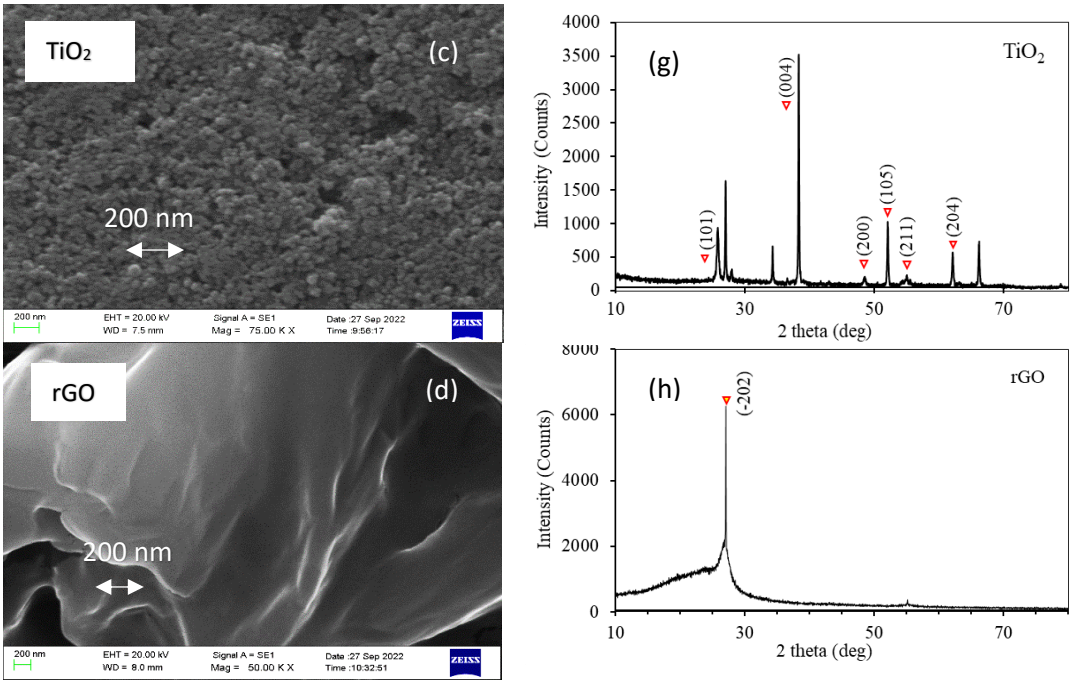

Figure 1. (a-d) Scanning electron micrographs (in 200 nm scale) and (e-h) XRD spectrums of electrodeposited ZnO and Cu_2O thin films, and doctor-bladed TiO_2 and rGO films fabricated on FTO substrates.

Considering their respective preferential orientations and other prominent Cu2O planes contributing to its polycrystalline nature, the average crystallite sizes (D) of the SMO were calculated using Debye Scherrer formula (Eq.1). Where 'λ' is the wavelength of X-ray (0.1541 nm), 'β' is FWHM (full width at half maximum), 'θ' is the diffraction angle and 'D' is the crystallite diameter of the film. According to the theory of grain-size dependence of film sensitivity/conductance, smaller grain size results in higher sensitivity as a gas sensor (Bochenkov & Sergeev, 2010)

$$D = \frac{0.9\,\lambda}{\beta \cos\theta} \tag{1}$$

Referring to the average crystallite size and inter-planer spacing values of Cu2O, ZnO, TiO2, and rGO thin film given in Table 1, the smallest crystallite size of ~ 42.8 nm was observed with Cu2O films which showcased a significant difference (~30 nm) with respect to other SMO grain sizes. Affirming a nano-structured thin film deposition, Cu2O can be identified as a potential candidate for efficient gas sensing, facilitating high grain-to-grain conduction and high surface area for gaseous content to get adsorbed. Meanwhile, the inter-planar spacing of Cu2O, ZnO, TiO2 crystalline planes showed a similar variation except for rGO, where the wrinkled sheets are accompanied with comparatively larger d-spacing of 0.329 nm.

Table 1. Average crystallite size (D) and inter-planar (d) spacing of Cu_2O, ZnO, TiO_2, and rGO thin films.

	Cu_2O	**ZnO**	**TiO_2**	**rGO**
Average inter planer spacing d (nm)	0.243	0.257	0.235	0.329
Crystallite size D (nm)	42.8	70.1	87.8	85.3

3.2 Advanced Optical and Electrical Characteristics

In order to interpret the electrical characteristic of SMO film surface, the AC impedance spectroscopy was carried out by placing two identical FTOs on top of the fabricated film with 1 mm distance apart. The Nyquist plots drawn in 1000 Hz – 1 MHz frequency range at zero bias are shown in Fig. 2(a-d) with curve fit and simulated ($\chi^2 \sim 0.01$) equivalent circuits of each film is given in the corresponding insets. In the equivalent circuit, RS represents the series resistance accompanied with FTO-SMO ohmic contacts. R1 and R2 are resistances that form parallel circuits with constant phase elements (CPE). RW indicates a Warburg impedance. The presence of CPE indicates porosity and surface roughness of the films.

The Nyquist curves of Cu2O and TiO2 depict deformed semi-circles which are attributed to the respective charge transfer process of the films at high frequencies. Further, in low frequency ranges, Cu2O and ZnO showed incomplete arcs whilst TiO2 showed a straight tail denoting an ionic conduction. Here, capacitive/inductive characteristics of Cu2O, ZnO, and TiO2 at low frequencies which are reflected by the presence of increasing imaginary component of the impedance (Kuwabara et al., 2009; Manjakkal et al., 2015). When comparing the curve height which denotes the total impedance, it was identified that rGO given in Fig. 2d displays a less capacitive/inductive and high conductive (low impedance) behavior.

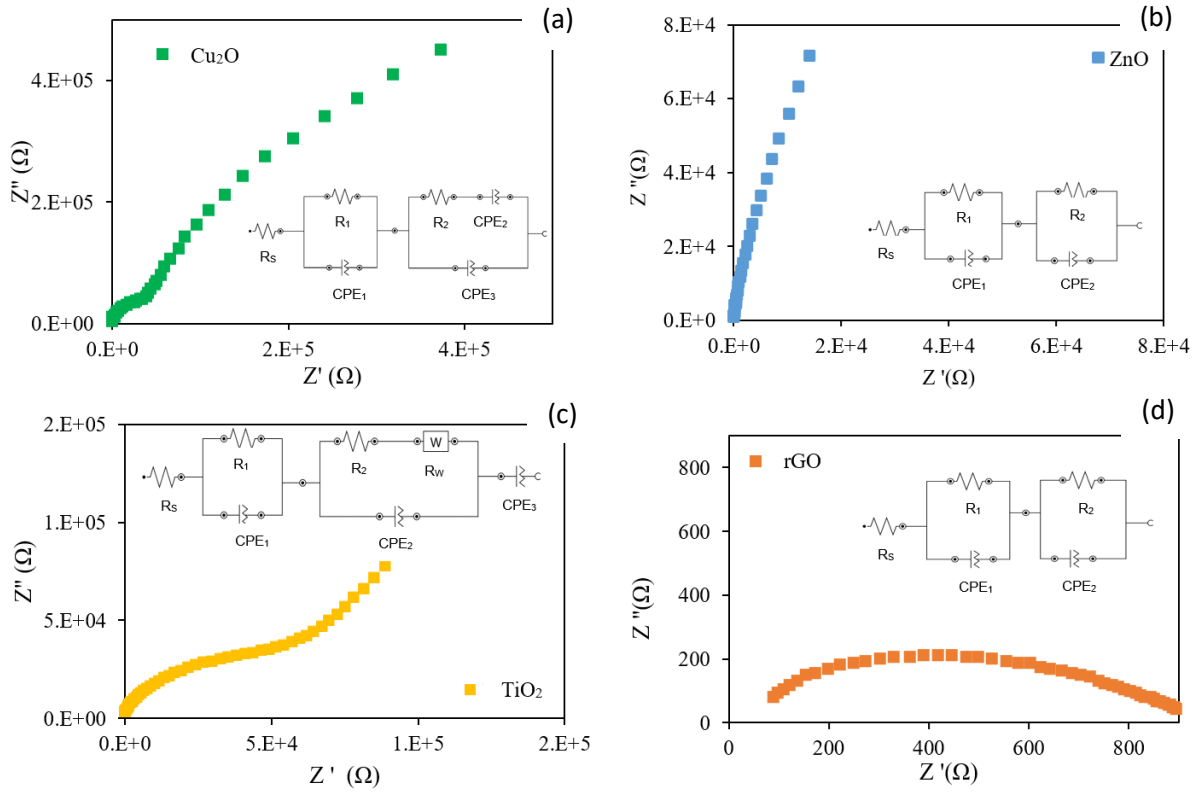

Figure 2. The Nyquist plot comparison between (a) Cu_2O, (b)ZnO, (c)TiO_2, and (d) rGO thin films. Insets shows the curve fit and simulated ($\chi^2 \sim 0.01$) equivalent circuits of each film.

Positive biasing voltage has been observed to decrease the complex impedances of SMO films as depicted in Fig. 3. TiO2 notably displays a reducing ionic conduction and increase in capacitive nature with forward biasing at low-frequency ranges. These findings suggest that the application of a positive biasing voltage alters the electrical properties of SMO films, with distinct behaviors observed in terms of impedance and capacitive characteristics, which are likely attributed to variations in their composition and structure.

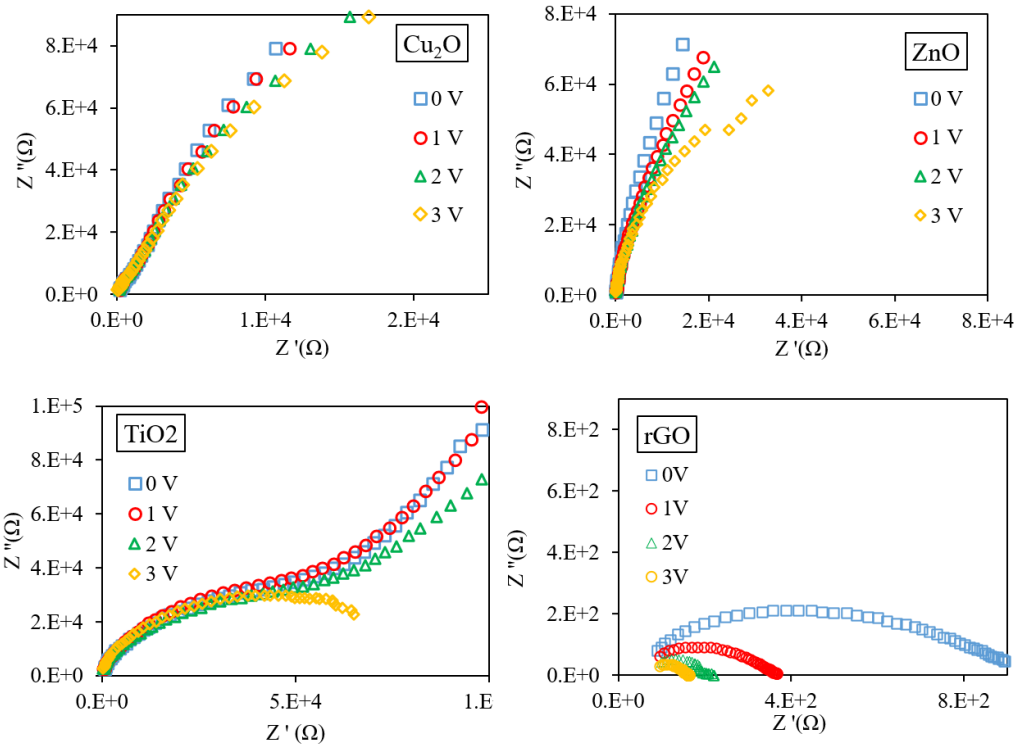

Figure 3. Nyquist plot comparison of complex impedance variations of Cu2O, ZnO, TiO2, and rGO thin films under positive biasing potentials of 0 V, 1 V, 2 V, and 3V.

A comparative analysis of the UV-visible absorption spectra of SMO thin films was carried out by film suspension method under a 200-800 nm wavelength range. Determined by Tauc's equation (Eq.2); where $\propto$ is the absorption coefficient for a certain wavelength, h is Planck's constant, Eg is the band gap, A is an energy independent coefficient which is 1 under general conditions (Sil et al., 2018) and υ is the frequency of incident photon where hυ gives the photons' energy the optical energy band gap variation was investigated among Cu2O, ZnO, TiO2, and rGO.

$$\alpha h\upsilon = A(h\upsilon - E_g)^{\frac{1}{2}} \tag{2}$$

The extrapolation of the linear region determines the direct band gaps of SMO, from the plot drawn $(\boldsymbol{\alpha h\upsilon})^2$ against the photon energy $\boldsymbol{h\upsilon}$. Fig 5 shows the Tauc plots and the corresponding optical direct bandgap values of Cu2O, ZnO, TiO2, and rGO. The respectively recorded band edge values of 2.5, 3.2, 3.3, and 1.9 electron-volts (eV) are in concordance with the literature (Bandara et al., 2017; Garrafa-Gálvez et al., 2019; Kumar et al., 2019). However, the other absorption bands identified in these films may be ascribed to the electronic transition across direct band gaps at unevenly deposited thicknesses of the films (Kumar et al., 2019) and the intermediate energy levels.

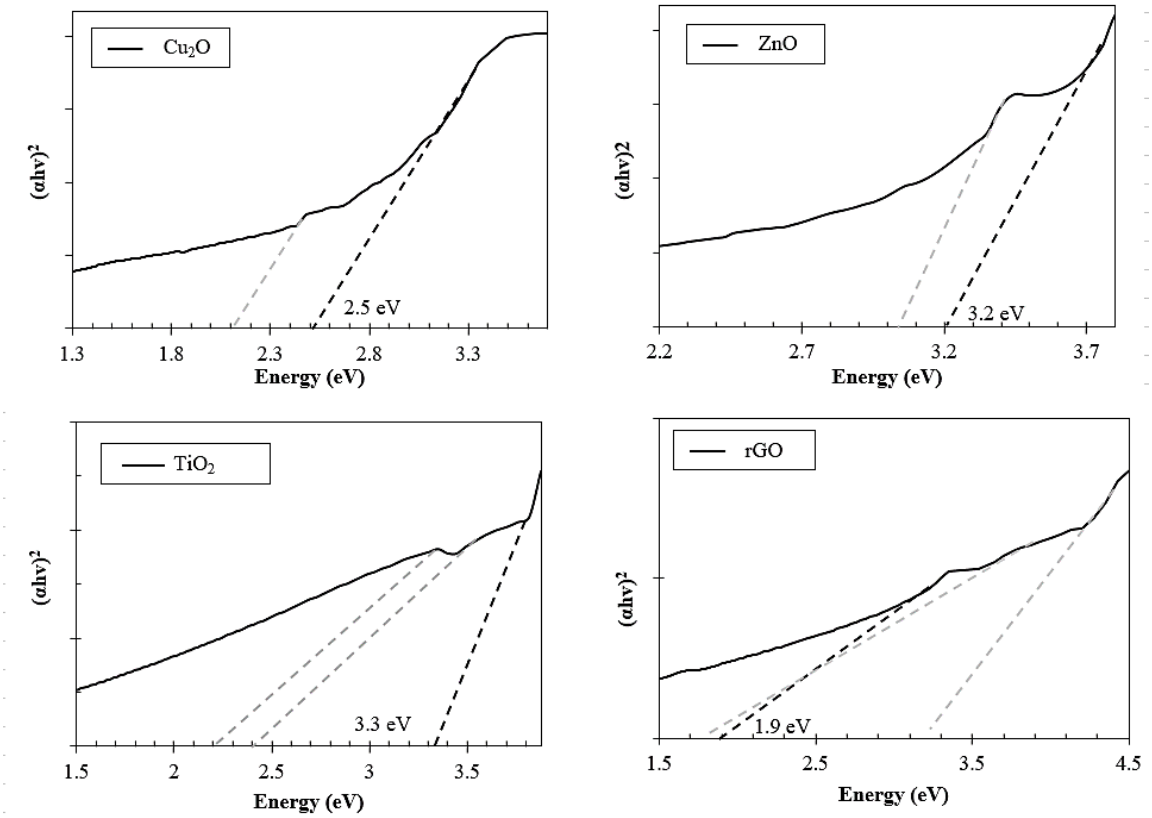

Figure 4. Tauc's plot of UV visible absorption spectra of Cu_2O, ZnO, TiO_2, and rGO thin films grown on FTO

3.3 LPG sensing

The gas sensing quality differences of SMO films were experimented with using LP gas that was injected into a sealed chamber with 5 cc min-1 constant flow rate which was flushed away with a constant 0.1 l min-1 compressed air flow before and after every cycle. Just before LP gas flowed into the chamber, it was passed through a silica background to absorb water molecules passing through the chamber. The temperature of the chamber was controlled at 70 ℃ and a settled film resistance at this ambient level (R_a) was obtained. In the presence of 5 cc min-1 constant LP gas (R_g) flow, the resistance change was observed to decrease or increase with the corresponding film (Bandara et al., 2023; Siripala et al., 1989). The time to reach 90% of the maximum resistance change (ΔR) caused due to LPG was undertaken as the films' response time and the time taken to return to 90% of the initial resistance under compressed airflow as the recovery time of the sensor. In general, p-Cu2O contains acceptor levels that are fully filled with electrons (ionized), near the valance band that remains with holes and n-Cu2O contains donor levels near its conduction band. At the ambient state, oxygen molecules in dry air are ionosorbed on the surface of the SMO films (Wang et al., 2017; Wang et al., 2018) Depending on the surface nature, temperature, and atmospheric conditions, this chemisorbed oxygen acquire the electrons from these trapped surface states of SMO and converts to molecular O2-, atomic O- and O2- (Eq.3-6).

$$O_{2(g)} \rightarrow O_{2(ads)} \quad (3)$$

$$O_{2(ads)} + e^- \rightarrow O_{2(ads)}^- \quad (4)$$

$$O_{2(ads)}^- + e^- \rightarrow 2O^- \quad (5)$$

$$O^- + e^- \rightarrow O^{2-} \quad (6)$$

The result is band bending, which forms a potential barrier at the surface called surface charged layer (SCL). As the hole concentration increases near the interface with p-type SMO, film resistance decreases increasing the electrical conductance in the film and stabilizing with time. With n-type SMO, film resistance decreases with time and come to stabilized level (Ra, ambient level). Upon the injection

of a reducing gas like LPG, it gets adsorbed on the SMO surface and interacts with the ionosorbed oxygen by forming gaseous species and water vapor as expressed in Eq.7. Thus, in the presence of LPG, surface trapped electrons get released and start recombining with holes. Hence, sensor resistance increases when film is p-type and decreases if n-type, signaling a gas response.

$$O^{2-} + C_nH_{2n+2} \rightarrow CO_2 + H_2O + 2e^- \quad (7)$$

The size dependence of gas sensitivity is explained in recent studies on the gas sensitivity of nanostructured metal oxides (Bochenkov & Sergeev, 2010) which suggest an increase in sensitivity when the grain size (D) is less than twice the thickness of the surface charge layer (L). Thus, a higher grain contribution has been observed in forming the space charge layer that exhibits greater change in film electronic conduction. On the other hand, smaller grains' dimensions lead to an enhanced surface area to volume ratio which enables efficient LPG interactions. LPG (100%) response of SMO films under 70 ℃ operating temperature are given in Fig.5. The resistance of the Cu2O sensor increased upon exposure to LPG (R_g), demonstrating p-type SMO behavior. Whilst TiO2, ZnO, and rGO displayed an n-type SMO behavior with decreasing film resistance with LPG exposure. The percentage change in the gas response compared to sensor resistance at ambient state (R_a) is given by Eq.8. For p-type Cu2O films $R_g > R_a$ and for n-type TiO2, ZnO, and rGO films $R_g < R_a$.

$$S = \left[\frac{(R_g - R_a)}{R_a}\right] \times 100\% \quad (8)$$

ZnO showed the highest LPG response of 27% with a considerably low response time of ~ 20 s. It was suspected that the long recovery period required by ZnO originated from its highly porous nature, which could delay the gas desorption process. Cu2O on the other hand showed significantly stable yet a not-so-high gas response under moderate response and recovery times of ~30 s and ~20 s. The low energy band gap of 2.5 eV observed with Cu2O facilitates a possibility to enhance the films' gas sensitivity at low operating temperatures, under light illumination; by increasing the electron/hole capability to overcome the surface potential barrier during the gas adsorption process with an expected increase in the LPG response rate.

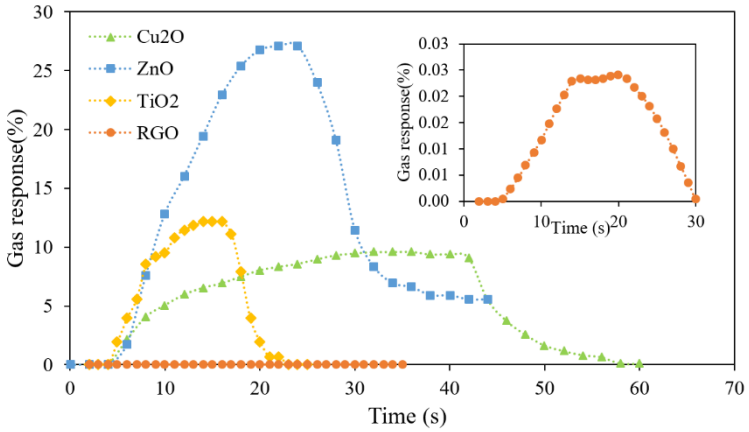

Figure 5. LPG response (%) comparison at 70 ℃ of Cu_2O, ZnO, TiO_2, and rGO thin films grown on FTO substrates. Inset signifies the rGO gas sensitivity.

4 CONCLUSION

The study investigated the relationship between the structure, morphology, and electrical properties of four different nanostructured SMOs such as Cu2O, ZnO, TiO2, and rGO, synthesized via electrochemical deposition and doctor blading technique, on their LPG sensing performance. XRD and SEM discovered material formation with increasing crystallite size observed for Cu2O (42.8 nm), ZnO (70.1 nm), and TiO2 (87.8 nm). Cu2O exhibited a dominant (111) phase with a cuboid morphology, while rGO displayed a single-plane (002) structure with a crumpled paper-like texture, indicating successful GO reduction. UV-vis analysis revealed distinct band gaps for ZnO (3.2 eV), TiO2 (3.3 eV), and rGO (1.9 eV), with Cu2O having the lowest (2.5 eV) and potential for enhanced photocatalytic activity as UV light-irradiated gas sensing. AC impedance measurements showed an increased film conductivity of SMOs with a positive bias. The advantages of nano-grain sizes, specific surface morphologies, and impedances of SMO in gas sensitivity were tested with LPG. Notably, ZnO films exhibited the highest gas response (~27%) for LPG at 70°C with fast response and recovery times (<20 seconds). Conversely, Cu2O displayed a stable and good sensitivity (~11%) towards LPG, potentially due to its smaller grain size. Continuing with the study, the UV and voltage-biased conditions are being identified to provide substantial results with LPG sensing. These findings highlight the importance of tailoring the structural, morphological, and electrical properties of SMOs for optimizing LPG sensing performance.

5 ACKNOWLEDGEMENTS

We would like to offer our sincere gratitude to the Open University of Sri Lanka for facilitating this research, all the authors for their contribution, support, and insightful feedback throughout the research process. We extend our appreciation to our families and friends for their unwavering support and encouragement throughout this project and to all those who have directly or indirectly supported this research.

REFERENCES

Bandara, A. H. M. N. N., Perera, V. P. S., Senadeera, G. R., & Bandara, K. D. (2023). Performances of Nano-Structured Cu2O Thin Films Electrochemically Deposited on ITO Substrates in Lactate Bath as Liquid Petroleum Gas Sensors. *ECS Advances*, *2*(4), 046501. https://doi.org/10.1149/2754-2734/ad040a

Bandara, K. N. D., Jayathilaka, K. M. D. C., Gunewardene, M. S., Dissanayake, D. P., & Jayanetti, J. K. D. S. (2017). Surface properties of sulphur based surface modified n-Cu2O thin films for enhanced liquefied petroleum gas sensing. *Journal of Physics D: Applied Physics*, *50(48)*, 485304. https://doi.org/10.1088/1361-6463/aa9204

Barreca, D., Comini, E., Ferrucci, A. P., Gasparotto, A., Maccato, C., Maragno, C., ... & Tondello, E. (2007). First example of ZnO− TiO2 nanocomposites by chemical vapor deposition: structure, morphology, composition, and gas sensing performances. *Chemistry of Materials*, *19(23)*, 5642-5649. https://doi.org/10.1021/cm701990f

Bochenkov, V. E., & Sergeev, G. B. (2010). Sensitivity, selectivity, and stability of gas-sensitive metal-oxide nanostructures. *Metal oxide nanostructures and their applications*, *3*, 31-52.

Chen, K., Wang, X., Xia, P., Xie, J., Wang, J., Li, X., ... & Li, L. (2020). Efficient removal of 2, 2′, 4, 4′-tetrabromodiphenyl ether with a Z-scheme Cu2O-(rGO-TiO2) photocatalyst under sunlight irradiation. *Chemosphere*, *254*, 126806. https://doi.org/10.1016/j.chemosphere.2020.126806

Choi, M. S., Kim, M. Y., Mirzaei, A., Kim, H. S., Kim, S. I., Baek, S. H., ... & Lee, K. H. (2021). Selective, sensitive, and stable NO2 gas sensor based on porous ZnO nanosheets. *Applied Surface Science*, *568*, 150910. https://doi.org/10.1016/j.apsusc.2021.150910

Garrafa-Gálvez, H. E., Alvarado-Beltrán, C. G., Almaral-Sánchez, J. L., Hurtado-Macías, A., Garzon-Fontecha, A. M., Luque, P. A., & Castro-Beltrán, A. (2019). Graphene role in improved solar

photocatalytic performance of TiO2-RGO nanocomposite. *Chemical Physics*, *521*, 35-43. https://doi.org/10.1016/j.chemphys.2019.01.013

Han, G., Lu, Q., Liu, G., Ye, X., Lin, S., Song, Y., ... & Li, G. (2012). Enhanced ethanol sensing properties based on α-Fe 2 O 3/In 2 O 3 hollow microspheres. *Journal of Materials Science: Materials in Electronics*, *23*, 1616-1620. https://doi.org/10.1007/s10854-012-0638-4

Ibrayev, N., Zhumabekov, A., Ghyngazov, S., & Lysenko, E. (2019). Synthesis and study of the properties of nanocomposite materials TiO2-GO and TiO2-rGO. *Materials Research Express*, *6(12)*, 125036. https://doi.org/10.1088/2053-1591/ab51a3

Kalubowila, K. D. R. N., Jayathileka, K. M. D. C., Kumara, L. S. R., Ohara, K., Kohara, S., Sakata, O., ... & Jayanetti, J. K. D. S. (2019). Effect of bath pH on electronic and morphological properties of electrodeposited Cu2O thin films. *Journal of The Electrochemical Society*, *166(4)*, D113. https://doi.org/10.1149/2.0551904jes

Kumar, V., Sharma, H., Singh, S. K., Kumar, S., & Vij, A. (2019). *Enhanced near-band edge emission in pulsed laser deposited ZnO/c-sapphire nanocrystalline thin films. Applied Physics A, 125(3).* https://doi.org/10.1007/s00339-019-2485-0

Kuwabara, T., Kawahara, Y., Yamaguchi, T., & Takahashi, K. (2009). Characterization of inverted-type organic solar cells with a ZnO layer as the electron collection electrode by ac impedance spectroscopy. *ACS applied materials & interfaces*, *1(10)*, 2107-2110. https://doi.org/10.1021/am900446x

Liao, L., Zhang, Z., Yan, B., Zheng, Z., Bao, Q. L., Wu, T., ... & Yu, T. (2009). Multifunctional CuO nanowire devices: p-type field effect transistors and CO gas sensors. *Nanotechnology*, *20(8)*, 085203. https://doi.org/10.1088/0957-4484/20/8/085203

Manjakkal, L., Cvejin, K., Kulawik, J., Zaraska, K., Szwagierczak, D. and Stojanovic, G. (2015) Sensing mechanism of RuO2–SnO2 thick film pH sensors studied by potentiometric method and electrochemical impedance spectroscopy. *Journal of Electroanalytical Chemistry*, *759*, 82-90. https://doi.org/10.1016/j.jelechem.2015.10.036

Miremadi, B. K., Singh, R. C., Chen, Z., Morrison, S. R., & Colbow, K. (1994). Chromium oxide gas sensors for the detection of hydrogen, oxygen and nitrogen oxide. *Sensors and Actuators B: Chemical*, *21(1)*, 1-4. https://doi.org/10.1016/0925-4005(93)01208-L

Musa, A. O., Akomolafe, T., & Carter, M. J. (1998). Production of cuprous oxide, a solar cell material, by thermal oxidation and a study of its physical and electrical properties. *Solar Energy Materials and Solar Cells*, *51(3-4)*, 305-316. https://doi.org/10.1016/S0927-0248(97)00233-X

Shishiyanu, S. T., Shishiyanu, T. S., & Lupan, O. I. (2005). Sensing characteristics of tin-doped ZnO thin films as NO2 gas sensor. *Sensors and Actuators B: Chemical*, *107(1)*, 379-386. https://doi.org/10.1016/j.snb.2004.10.030

Sil, S., Dey, A., Datta, J., Das, M., Jana, R., Halder, S., ... & Ray, P. P. (2018). Analysis of interfaces in Bornite (Cu5FeS4) fabricated Schottky diode using impedance spectroscopy method and its photosensitive behavior. *Materials Research Bulletin*, *106*, 337-345. https://doi.org/10.1016/j.materresbull.2018.06.016

Siripala, W., & Kumara, K. P. (1989). A photoelectrochemical investigation of the n-and p-type semiconducting behavior of copper (I) oxide films. *Semiconductor science and technology*, *4(6)*, 465. https://doi.org/10.1088/0268-1242/4/6/007

Wang, P., Wang, J., Wang, X., Yu, H., Yu, J., Lei, M., & Wang, Y. (2013). One-step synthesis of easy-recycling TiO2-rGO nanocomposite photocatalysts with enhanced photocatalytic activity. *Applied Catalysis B: Environmental*, *132*, 452-459. https://doi.org/10.1016/j.apcatb.2012.12.009

Wang, P., Zhan, S., Xia, Y., Ma, S., Zhou, Q., & Li, Y. (2017). The fundamental role and mechanism of reduced graphene oxide in rGO/Pt-TiO2 nanocomposite for high-performance photocatalytic water splitting. *Applied Catalysis B: Environmental*, *207*, 335-346. https://doi.org/10.1016/j.apcatb.2017.02.031

Wang, X. F., Song, X. Z., Sun, K. M., Cheng, L., & Ma, W. (2018). MOFs-derived porous nanomaterials for gas sensing. *Polyhedron*, *152*, 155-163. https://doi.org/10.1016/j.poly.2018.06.037